Agricultural and Forest Meteorology 208 (2015) 40–49

Contents lists available at ScienceDirect

Agricultural and Forest Meteorology

journal homepage: www.elsevier.com/locate/agrformet

Novel forest structure metrics from airborne LiDAR data for improved snow interception estimation

D. Moeser[a,b,*], F. Morsdorf[c], T. Jonas[a]

[a] WSL Institute for Snow and Avalanche Research SLF, Davos Dorf, Switzerland
[b] Forest Ecology, Institute of Terrestrial Ecosystems, Department of Environmental Sciences, Swiss Federal Institute of Technology ETH, Universitätstrasse 16, CH-8092 Zurich, Switzerland
[c] Remote Sensing Laboratories, Department of Geography, University of Zurich, Switzerland

ARTICLE INFO

Article history:
Received 18 November 2014
Received in revised form 7 April 2015
Accepted 19 April 2015
Available online 2 May 2015

Keywords:
Aerial LiDAR
Snow interception
Forest snow modeling
Canopy metrics
LAI
Canopy closure

ABSTRACT

A set of 57 novel canopy metrics of potential value for snow modeling were created from airborne LiDAR data. The metrics were meant to estimate size and relative location of gap openings around a point within forested areas, allowing for measures of the spatial arrangement of surrounding canopy elements. These new metrics were correlated with snow interception measured in the field (8488 manually measured snow interception points). The results were further compared to the correlation values between effective interception and traditionally used forest parameters (CC and LAI). The correspondence between all metrics was also analyzed in order to understand the potential cross correlation between each variable. LAI (average *R*: 0.57) demonstrated low correlations when directly compared to snow interception and further showed a large cross correlation with canopy closure (average *R*: 0.72). A new metric, 'mean distance to canopy' had the highest correlation (average *R*: 0.78) over all storm events to the effective interception. But in contrast to LAI, this metric did not show any cross correlation with canopy closure (CC). Likewise, 'total gap area,' an indirect measurement of apparent gap fraction (another new metric), also showed a high correlation to effective interception (average *R*: 0.72) without demonstrating a significant cross correlation to CC or to mean distance to canopy. These findings suggest that modeling forest snow processes with both CC and LAI may not be the best option due to both the low correlation of LAI as well as high cross correlation between these parameters. However, the pairing of mean distance to canopy and/or total gap area with canopy closure could give more robust estimations of snow interception within heterogeneous terrain.

1. Introduction

The hydrology of forests plays an important role in the global water budget. Snowmelt dominated watershed headwaters which contain forests produce 60% of the global freshwater runoff (Chang, 2003). Forest canopy structure greatly influences snow accumulation and melt and controls water availability from forested areas. Specifically, the surrounding forest structure can influence involved physical processes, creating much greater spatial snow pack heterogeneity compared to open areas. Snow interception, a major driver of heterogeneous snow distribution, ranges from low to just over 60% of total annual snowfall (Montesi et al., 2003; Storck et al., 2002).

The importance of snow interception within forest canopies has not gone unnoticed within the hydrology community. There is a growing body of work spanning 75 years which described attempts to directly quantify and model forest snow interception (Hedstrom and Pomeroy, 1998; Satterlund and Haupt, 1967; Schmidt and Gluns, 1991; Varhola et al., 2010b). These studies highlight the complex interplay between the physical under-canopy energy and water balance processes and the overhead multidimensional arrangement of forest canopy characteristics. Intercepted snow on the forest canopy drives sublimation in forested areas and like interception, sublimation is highly variable. Many studies have estimated sublimation from coniferous canopies to range from 25 to 50% of the total annual snowfall in cold and dry climates typical of the northern boreal forests (Essery and Pomeroy, 2001; Essery et al., 2003; Hedstrom and Pomeroy, 1998; Lundberg and Halldin, 2001). Interception in many cases represents water

* Corresponding author at: WSL Institute for Snow and Avalanche Research SLF, Fluelastrasse 11, CH-7260 Davos Dorf, Switzerland. Tel.: +41 81 4170 156; fax: +41 81 4170 0110.
E-mail addresses: moeser@slf.ch (D. Moeser), felix.morsdorf@geo.uzh.ch (F. Morsdorf), jonas@slf.ch (T. Jonas).

http://dx.doi.org/10.1016/j.agrformet.2015.04.013
0168-1923/

lost (due to sublimation) to not only local water balances, but to larger-scale water budgets. Within the Northern Hemisphere it is estimated that 20% of the seasonal snow cover is located within forested areas and can account for 17% of total terrestrial water storage during the winter season (Guntner et al., 2007; Rutter et al., 2009).

Due to the recognized importance of forest snow processes on the water budget, many snow models include a vegetative canopy representation. The Snow Model Inter-comparison Project (SnowMIP2) included 33 models with a canopy representation of varying degrees of complexity (Essery et al., 2009; Rutter et al., 2009). All of these models, which have directly integrated a snow interception module, utilize either canopy closure (CC), leaf area index (LAI) or a composite of the two to describe the canopy structure. However, the interplay between canopy characteristics such as LAI and CC and snow interception also depends on where these characteristics are situated in relation to the greater surrounding forest architecture.

Canopy gaps have large impacts on the snow holding capacity in many forested areas. These areas can show divergent snow accumulation patterns as compared to the surrounding forest and can house maximum snow accumulation even as compared to neighboring open areas (Troendle and Meiman, 1986; Winkler et al., 2005). The interfaces between the open and forested areas also show the most heterogeneous snow accumulation and ablation patterns within a forested area and can house both the maxima and minima snow depths depending upon the position relative to the surrounding forest (Golding and Swanson, 1986; Veatch et al., 2009). In efforts to describe the relationship between openness and surrounding canopy, some practitioners categorize gaps for opening size as a function of the average surrounding tree size. In order to permit for more robust interception modeling at landscape scales, the greater canopy topography as well as the spatial heterogeneity of canopy structure needs to be accounted for within the models. Despite this, interception modules continue to use only point based predictors, most likely due to the intensive requisite time involved in collecting canopy metrics over large areas.

Standard overhead canopy structure methods for measurement are prohibitively labor intensive and normally require destructive sampling of the overstory. However, there are many indirect methods which include hemispherical photography, plant canopy analyzers (LAI-2000), or a spherical densitometer and each have particular strengths and weaknesses (Breda, 2003; Hyer and Goetz, 2004). Hemispherical photography (HP) is increasingly becoming a standard method for canopy structure characterization. However, this technique can deliver a broad range of estimates dependent upon the initial camera and utilized program settings and allows for derivations of only point based CC, LAI and incoming shortwave radiation on the forest floor (Zhang et al., 2005). HP image acquisition and processing, like the other field methods, is also very time consuming, thus limiting the utility of accurately describing these metrics for large areas.

Airborne laser scanning (ALS) data has been increasingly utilized to derive estimates of CC and LAI with good correlations and is becoming more readily available for large areas throughout the world (Asner et al., 2011; Fleck et al., 2012; Korhonen and Morsdorf, 2014; Lovell et al., 2003; Moeser et al., 2014; Morsdorf et al., 2006, 2004; Riaño et al., 2004; Solberg, 2010; Solberg et al., 2009). ALS can also derive large scale features such as canopy openings within forested areas and it is also possible to provide information on how these open areas are positioned relative to the surrounding forest.

Since ALS can quickly characterize surfaces over large scales, it can also be used for a variety of novel canopy metric estimates of potential value for forest snow modeling. As outlined above, such investigations represent a significant research gap with large potential improvements within forest hydrology, which have just begun to be investigated (Varhola et al., 2010a; Zhao et al., 2011). While the aim is to find metrics specifically related to snow interception, it is possible that there could be overlap from these findings into other disciplines such as forest ecology and biology, where such metrics have not yet been fully investigated.

This analysis was done in order to better answer the following questions: Should we be using LAI and CC as the primary canopy descriptors within forest snow models? Are there more robust canopy descriptors which could be utilized? This work has highlighted the utility behind the algorithm used for the calculation of new canopy metrics and tested their functionality. We created 57 canopy metrics from ALS data of potential value for snow modeling. The variables were meant to estimate size and relative location of gap openings around a point within a forested area, allowing for measures of the spatial arrangement of surrounding canopy elements. These new metrics were directly correlated snow interception measured in the field (8488 manually measured snow interception points). The results were further compared to the correlation values between interception and the traditional parameters (CC and LAI), as well as incoming shortwave radiation estimates. The correspondence between all metrics was also analyzed in order to understand the potential cross correlation between each parameter.

2. Methods

2.1. Field areas

Seven forested field areas were equipped for a multiyear study in the region immediately surrounding Davos, Switzerland (Fig. 1). The field areas were 50 m × 50 m, and were chosen due to the highly heterogeneous canopy coverages at the sub-plot scale along with larger scale canopy characteristics such as open areas present within the 'medium' and 'low' sites (Fig. 1). Forest stands were predominately Norwegian spruce and varied in height from new growth up to 45 m in height with the majority between 10 and 30 m. Within each field area were 276 pre-labeled and surveyed points with a maximum absolute positioning error of ±50 cm (derived from 36 control measurements within each field area) for a total of 1932 locations for repeated ground measurements. Each sampling grid was arranged in the same setup within all field areas (Fig. 1). Two open field areas were further equipped as reference sites for direct comparison to the under canopy snow measurements (refer to Moeser et al., 2014 for a more detailed description).

2.2. Snow data collection

Snow depth data was collected after every snow storm event (defined here as a total open area snowfall amount of 15 cm or greater) in the winter 2012 and 2013 season (15 cm threshold dictated by the IMIS–SLF meteorological station from the intercantonal measurement and information system). These depth measurements were collected at each forested point (1932 points) as well as at 100 open area control points (total of 69,552 measurements). Snow interception however was measured after only 9 of these snowfall events (from a total of 27) due to the demanding pre-conditions necessary for such a campaign: (1) forest canopy 100% snow free before a snow storm event, (2) a defined crust on the underlying snow, and (3) minimal wind redistribution during the storm period. When all of these pre-conditions were met, a differential snow depth was measured immediately after snowfall, i.e., the new snow accumulated on top of the overlying crust. From these pre-conditions, the measurements can be thought of as 1 – snow interception. After parsing all snow measurements and removing all data potentially conflicting with the pre-conditions

there were 8488 remaining interception measurement points available for comparison. Despite the initial data parsing and the pre conditions, it is likely the data contains intra storm period unloading events when the maximum interception capacity above a measurement point is reached. Due to this, the interception measurements refer to effective interception (or cumulative storm interception). It is possible to attach an unloading estimate to these measurements from the work of Hedstrom and Pomeroy (1998), Pomeroy et al. (1998a,b); Pomeroy et al. (1998a,b) as well as Storck et al. (2002). However, these unloading metrics involve just an initial multiplier (0.678 and 0.6, respectively) regardless of the time step or overlying canopy, creating no change in the correlation between the interception measurements and the proposed canopy metrics. Furthermore, the only other unloading algorithms of which the authors are aware use a temperature threshold of 0 at which point the difference between the snow storage capacity of the tree and the rain storage capacity of the tree is given as unloaded snow (Koivusalo and Kokkonen, 2002). Since the temperature values are well below freezing, this algorithm would not account for the snow unloaded during the storms (Table 1).

All snow depth values were converted into snow water equivalent (SWE) from the US Army Corps of Engineers (1956) where snow density was related to the average storm temperature as follows:

$$\text{Snow density} = 67.92 + 51.25\, e^{(T/2.59)} \quad (1)$$

where T is the average storm air temperature (°C). The air temperature at each site, for each storm event, was interpolated from individual linear models created for each storm event with an average correlation coefficient of 0.92 and root mean square error of 0.38 (Fig. 2). Each temperature model utilized temperature data from 4 meteorological stations from the 'Intercantonal measurement and information system' (IMIS) surrounding Davos, Switzerland at four unique elevation bands: 1560 m, 2140 m, 2290 m, 2540 m (IMIS–KLO, IMIS–SLF, IMIS–PAR, IMIS–WFJ).

Eq. (1) was then used to attach fresh snow density values to all measured snow depth values at each storm to calculate SWE. Finally, the observed interception was derived from the difference between the freshly fallen SWE in the open and the freshly fallen SWE in the forest.

Table 1
Dates of snow sampling within the 2012/13 and 13/14 winter seasons. The snow depth measurements represent the total snow storm depth which fell in the Laret open field site. The swe and temperature, representing storm based values (swe – total storm swe, and temp – average storm temperature °C), are modeled for the Laret open field site. The wind speed is the average wind speed during each storm event at the Davos Stilli Meteorological station at 1560 m situated just south of the lake seen (and labeled) in Fig. 1.

Storm date	Snow depth (cm)	swe (mm)	Temp (°C)	Wind speed (m/s)
13-January-2013	28.53	22.65	−3.9	0.27
22-February-2013	20.31	13.89	−12.1	0.55
6-March-2013	37.16	28.96	−4.2	0.56
20-March-2013	16.81	13.62	−3.5	0.19
27-March-2013	17.41	12.81	−5.7	0.58
15-January-2014	27.65	24.42	−2.4	1.71
28-January-2014	27.80	21.18	−4.7	0.26
17-February-2014	24.31	22.49	−1.9	1.38
24-March-2014	35.88	26.93	−5.1	2.33

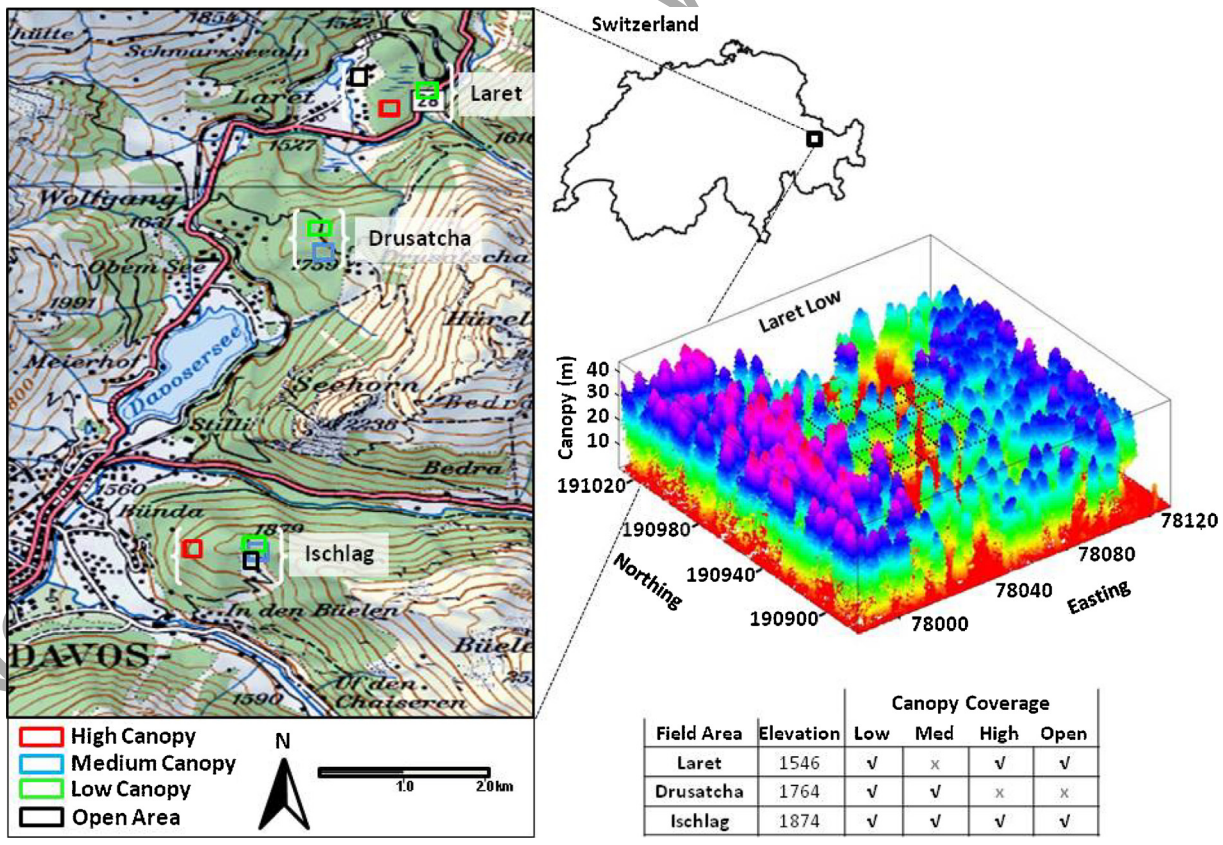

Field Area	Elevation	Canopy Coverage			
		Low	Med	High	Open
Laret	1546	√	x	√	√
Drusatcha	1764	√	√	x	x
Ischlag	1874	√	√	√	√

Fig. 1. There were seven forested areas and two open field areas located in three elevation regimes around Davos in eastern Switzerland. Each field area was located in a unique gap fraction regime and maintained heterogeneous canopy characteristics. The box plot on the right is a representation of the ALS cloud data within the Laret low field area. The sampling grid with each point (276 points), represented as black dots along the internal grid, can be seen within the ALS cloud box plot. The other field areas have the same experimental setup and the generalized canopy coverages and elevations for these areas can be seen in the lower right table.

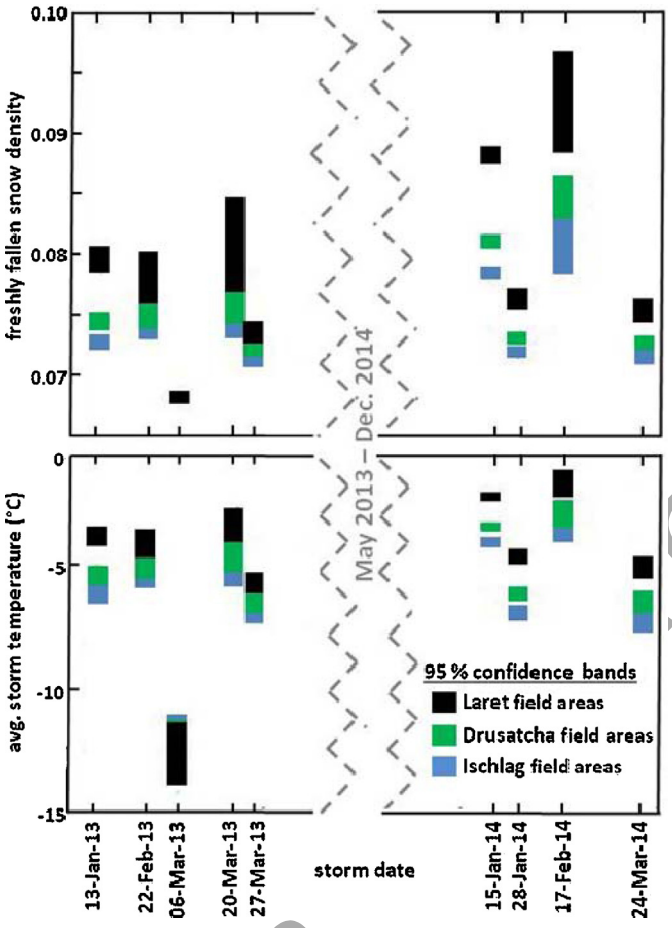

Fig. 2. Four meteorological stations surrounding Davos were used to create a linear temperature model unique to each time step to estimate temperature at each field area. These temperatures were then used to estimate the density of the freshly fallen snow at each field area for each storm using the algorithm from the US Army Corps of Engineers (1956). The confidence intervals for the density model utilize the confidence bounds from the temperature models. Note that the confidence bands within the density graph are minimal at low temperatures due to the exponential nature of the density model showing that despite large spread in confidence for the temperature during storm 3, this uncertainly was not transferred to the density model.

2.3. ALS data

2.3.1. Technical details

ALS data acquisition was carried out from 11th to 15th of September 2010 using a Riegl LMS Q 560 sensor from a series of helicopter flyovers at a nominal flying altitude of 700 m above the ground for a total area of ~90 km^2. The wavelength emitted from the Riegl device was 1550 nm with pulse durations of 5 ns and up to 7 returns were detected per pulse using a maximum scan angle of ±15°. Morsdorf et al. (2008) performed an experiment over similar terrain within similar conditions where it was showed that small scan angles do not significantly alter the measurements of canopy gap fractions. The post processing of the full waveform data set yielded an average echo density of 36 pulses per m^2 of the flyover domain and 19 pulses per m^2 for the last returns (i.e., shot density) within the utilized domain area. The affiliated digital terrain model (DTM) or the underlying ground surface elevations were computed by using the classified ground returns at a 0.5 m horizontal resolution by Toposys using their in house processing software, TopPit (http://www.toposys.com/).

2.3.2. CC, LAI and radiation flux derivation

Canopy closure, LAI (effective LAI) and incoming shortwave radiation was estimated from the ALS data by creation of synthetic hemispheric images at each ground point (1932 points) from conversion of the standard Cartesian *X,Y,Z* coordinate system to a polar system to mimic the angular viewpoint of a hemispherical photograph. These synthetic images were processed as if they were normal hemispherical photographs with 'Hemisfer', an image analysis software developed at the Swiss Federal Institute for Forest, Snow and Landscape Research WSL (http://www.wsl.ch/dienstleistungen/produkte/software/hemisfer/, Thimonier et al., 2010). Despite the limited scan angle of the flyover, these estimates showed high correlations ranging from $R = 0.83$ for LAI, $R = 0.93$ for CC (when compared to hemispherical photos) and $R = 0.90 - 09.4$ for incoming solar radiation (when compared to radiometer data) depending upon the site. Refer to Moeser et al. (2014) for a detailed method description.

2.3.3. Canopy metric definition

In addition to the standard metrics (CC and LAI), new canopy metrics were created at each ground point (1932 points). These metrics were generated from a vector searching algorithm designed to analyze ALS data for canopy characteristics which quantify the dimensions of a canopy gap at various directions as well as total gap size area. This section explains the basic functionality of the algorithm and gives general definitions of the new canopy metrics. Section 2.3.4 gives a detailed explanation of how the algorithm functioned.

The algorithm searched ALS data transformed into a 2 dimensional tree height model at specific user defined locations (i.e., the ground points). The data was scanned for the presence of canopy

elements in 192 unique directions (every 1.9°) on the planar surface from vectors originating at a predefined point. Each of the 192 directional vectors, with the origin at the user defined location, traveled in unique and constant directions until a canopy element was hit (end point). Each vector was then attached the distance (in meters) between the user defined location and the closest canopy feature which was in the directional path of the vector (Fig. 3). All end points from the 192 vectors were connected and a 2-dimensional poly-shape was created (Fig. 4c). This was repeated for all user defined locations. This poly-shape (total gap area) represented the size of the gap surrounding the user defined point(s) in m^2, or in other words the total open area around a point. The mean length of each directional vector (mean distance to canopy) in m, the max length of each vector (max distance to canopy), and the minimum length of each vector around from the user defined point (min distance to canopy) were also calculated which gave generalized information about the fetch of a canopy gap from the location perspective at the point in question, as well as the point(s) location relative to the gap.

Vector pairs were used in further calculations and were defined as the coupling of two opposing vectors (92 vector pairs). For example, the vector traveling exactly west from a point would be paired with the vector traveling exactly east. The mean length of the vector pairs were calculated (mean gap diameter) in m, along with the maximum (maximum gap diameter) and minimum vector pair lengths (minimum gap diameter) in order to provide basic information about the shape of the gap around the point in question.

All of these metrics were additionally generated for unique directional sectors, where the vector searching sectors were limited to 180 and 90° windows. The 180° windows included analyses restricted to the cardinal directions, north, south, east and west. The 90° windows included all quarter quadrants as well as the cardinal directions: north, south, east, west, northeast, southeast, southwest, and northwest. Refer to Table 2 for an overview of the calculated metrics. To use total gap area as an example; total gap area was calculated around the predefined points for the (1) entire domain (360°), (2) to the north with a 180° search window, (3) to the east with a 180° search window, (4) to the south with a 180°

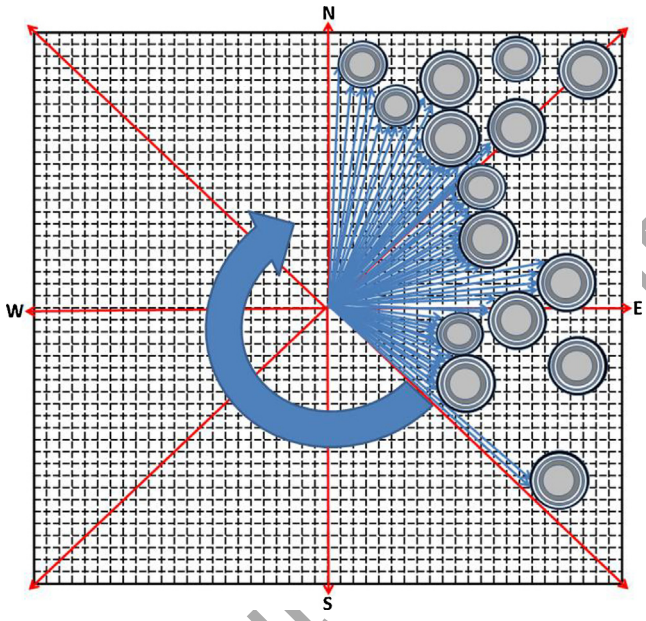

Fig. 3. Schematic of the searching vectors (blue) movement within an empty domain. Vectors begin and finish due north and move in a clockwise rotation. Red lines represent the breaks between the directional sectors. The underlying gridded domain is seen in the background. The vectors reach the edge of the domain unless a canopy element (represented as a dark circle) is first reached. (For interpretation of the references to color in this figure legend, the reader is referred to the web version of this article.)

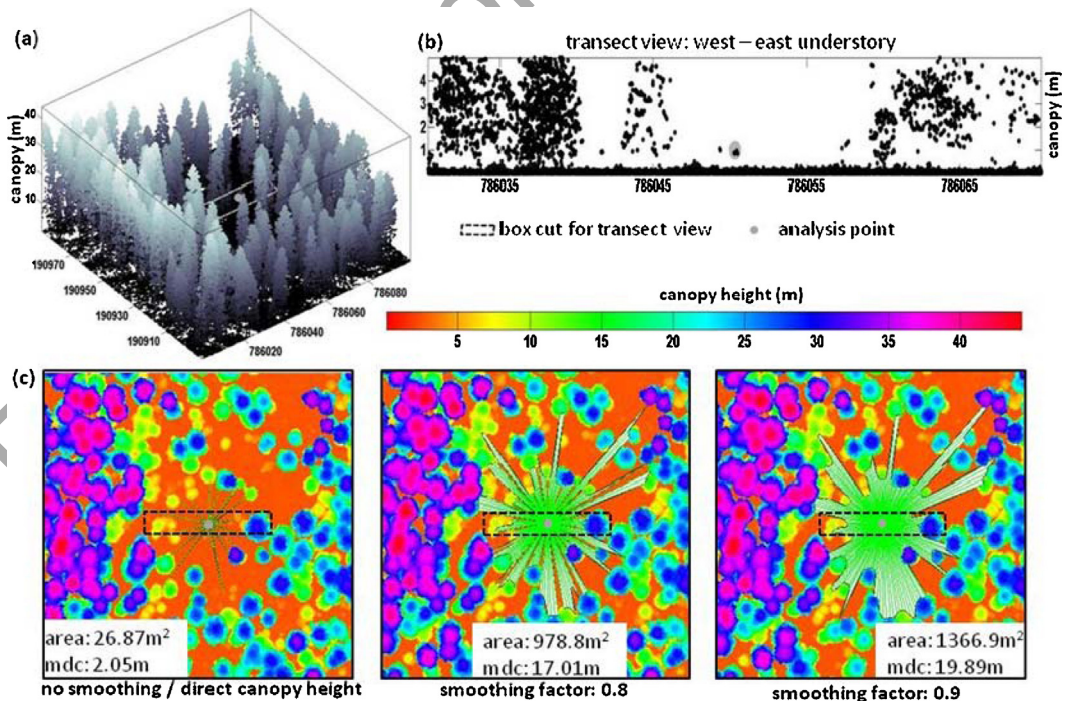

Fig. 4. (a) LiDAR point cloud data around measurement point 'C1' within the 'Laret low' field area. (b) Shows the understory of LiDAR returns (zoom in of canopy returns less than 5 m which were located within the box cut domain seen within each subsequent tile) with the analysis point at the established *h*th of 1.25 m. Please note lack of structure seen within the understory as compared to the overstory in part a. (c) 2-d viewpoints of the same data from part a. These tile show the polygon's created in green from 3 different smoothing scenarios. The estimated gap area (area) and mean dist to canopy (mdc) can be seen within the insets of each. Column three of (c) shows the best fit smoothing factor of 0.9. The black box within each plan view shows the exact dimensions of the transect view in part b. All utilize a starting box of 0.75 m and a height threshold of 1.25 m.

Table 2
Fifty-seven canopy metrics were created from the searching algorithm. Gap area and distance to canopy metrics were derived for the entire domain as well as for each directional sector from a 90 and 180° search window. The gap diameter metrics and canopy height proxies were generated only for the entire domain. Values within parentheses indicate number of times the descriptor was created.

Canopy descriptors	The full domain (360°)	180° sector (N,S, E, W)	90° sector (N,S, E, W,NE, SE,SW, NW)
Total gap area (m^2)	√	√ (4x)	√ (8x)
Max gap diameter (m)	√	–	–
Max distance to canopy (m)	√	√ (4x)	√ (8x)
Min gap diameter (m)	√	–	–
Min distance to canopy (m)	√	√ (4x)	√ (8x)
Mean gap diameter (m)	√	–	–
Mean distance to canopy (m)	√	√ (4x)	√ (8x)
Max canopy height proxy (m)	√	–	–
Mean canopy height proxy (m)	√	–	–

search window, (5) to the west with a 180° search window, (6) to north with a 90° search window, (7) to the northeast with a 90° search window, (8) to the east with a 90° search window, (9) to the southeast with a 90° search window, (10) to the south with a 90° search window, (11) to the southwest with a 90° search window, (12) to the west with a 90° search window, and (13) to the northwest with a 90° search window. The directional windows were also used for the mean distance to canopy, maximum distance to canopy and minimum distance to canopy metrics. The vector pair metrics (mean gap diameter, maximum gap diameter and minimum gap diameter) were only generated for the entire domain (360° window).

Finally, in addition to the directional searches, a secondary static domain with a 10 m radius around each point was then used to estimate general tree height proxies around the predefined points. A maximum canopy height value (max canopy height proxy) was calculated for each data trap as well as an average of all values within each data trap (mean canopy height proxy) from the tree height module. Table 2 outlines all calculated metrics.

2.3.4. Searching algorithm construction

The directional search for canopy elements surrounding a given center location utilized the general procedure outlined in the previous section. Specifically, an initial height threshold (*h*th), a starting bounding box where the vectors travel through despite potential presence of canopy elements, and a basic smoothing function were integrated into the algorithm to cope with unwanted scatter due to ungrouped understory canopy returns (Fig. 4).

When a height threshold is set, the algorithm ignores all canopy elements which have heights less than the pre-established value. The height threshold was set at 1.25 m in order to mimic settings that were also used for the derivation of the ALS based CC, LAI and incoming solar radiation (Moeser et al., 2014). Therefore the 192 vectors around the predefined point(s) only stop when a canopy element greater than the *h*th (1.25 m) within the direction path is reached.

The smoothing function was introduced in order to reduce the amount of noise effects of the ALS returns within the understory. Refer to Fig. 4 for a transect view of the understory surrounding a point. The smoothing function was implemented by creating a 0.25 × 0.25 m raster of the ALS data cloud where the average return value (transformed to canopy heights) was then assigned to each grid cell. This grid was then binarized based on the *h*th: When the gridded canopy returns were ≥*h*th (1.25 m), the grid cell value was assigned 1 and when the return was <*h*th (1.25 m), the grid cell value was assigned 0. A moving 3 × 3 neighborhood cell mean filter

Table 3
Overview of correlations of canopy metrics to interception ratio, where the mean represents correlations averaged over each storm event and stdev represents the standard deviation of the correlations. All values under each header are organized from high to low correlation. No maximum or minimum distance to canopy estimations are shown due to significantly lower correlations as compared to the mean distance estimates. Gap area diameter estimates were also removed due to near identical correlations shared with mean distance to canopy estimations.

Correlations to SWE interception at 9 storm events					
Searching function – distance			Searching function – area		
	Mean	stdev		Mean	stdev
Mean dist. to canopy	0.78	0.09	Total gap area	0.72	0.11
Mean dist. to canopy – north 180°	0.74	0.10	Total gap area – east 180°	0.67	0.11
Mean dist. to canopy – east 180°	0.74	0.09	Total gap area – north 180°	0.64	0.11
Mean dist. to canopy – south 180°	0.70	0.09	Total gap area – south 180°	0.64	0.10
Mean dist. to canopy – east 90°	0.70	0.09	Total gap area – east 90°	0.60	0.10
Mean dist. to canopy – NE 90°	0.69	0.09	Total gap area – NE 90°	0.59	0.09
Mean dist. to canopy – west 180°	0.68	0.09	Total gap area – west 180°	0.57	0.09
Mean dist. to canopy – north 90°	0.67	0.10	Total gap area – SE 90°	0.55	0.10
Mean dist. to canopy – SE 90°	0.64	0.09	Total gap area – south 90°	0.52	0.09
Mean dist. to canopy – NW. 90°	0.62	0.10	Total gap area – north 90°	0.50	0.10
Mean dist. to canopy – south 90°	0.62	0.08	Total gap area – SW 90°	0.50	0.08
Mean dist. to canopy – west 90°	0.61	0.08	Total gap area – NW 90°	0.49	0.11
Mean dist. to canopy – SW 90°	0.60	0.07	Total gap area – west 90°	0.48	0.08
Solar radiation			Standard metrics		
Mean daily DIF_IR**	0.74	0.12	Mean canopy height	0.72	0.08
Mean daily PISR**	0.67	0.14	Canopy closure**	0.72	0.13
Mean daily DIR_IR**	0.54	0.15	LAI**	0.57	0.16

'DIF_IR' represents the diffuse under canopy component of the estimated incoming solar radiation, 'DIR_IR' represents the direct under canopy component of the estimated incoming solar radiation and 'PISR' represents the potential incoming solar radiation or a composite of the direct and indirect component. While canopy closure maintains significant correlations please note the low LAI value of 0.57 (range 0.21–0.77) which demonstrated a 21% reduction as compared to the best correlated factor, mean distance to canopy (*R*: 0.78).

** Represents variables created using synthetic images.

was applied over the domain (200 m × 200 m domain around each analysis point) where each element *i*, situated in the middle of the neighborhood, was assigned the mean of the neighborhood.

The smoothing function was further parameterized by a smoothing factor which represented a percentage of canopy/percentage of total. The smoothing factor acted as secondary threshold within the smoothed raster and values above this threshold value were considered canopy and values below are passed through by the search vectors. This value was optimized to a value of 0.9 (the vector was stopped at a grid cell when at least 90% of the surrounding grid cells had canopy elements over the *h*th) based on a visual comparison with the ALS data cloud (Fig. 4c). From the use of this smoothing factor with the smoothed raster, the vectors were able to bypass ungrouped understory canopy returns, which allowed for the vectors to travel past canopy returns which fell over the *h*th (1.25 m) but demonstrated a low surrounding density (Fig. 4b).

Finally, since the smoothing function was based on a gridded approach, an initial starting bounding box was integrated. For example, if the neighboring pixel to the north of the starting point was classified as canopy, then entire 45° viewshed to the north would have also been classified as canopy, since all vectors traveling between the northwest and northeast directions would hit this grid cell. Due to this, an initial starting distance of 0.75 m was allocated to the searching vectors, which reduced the significance of canopy hits close to the starting point affecting the neighboring classifications.

2.3.5. Searching algorithm transferability

Since the vector searching algorithm works on ALS data converted to a raster, high point cloud density data is not necessarily needed to provide accurate metric derivation. This process has been fully automated and initial settings including the height threshold, the grid size of the raster (raster of ALS data cloud), smoothing factor and initial starting bounding box as well as the predefined location list (where the process was to be performed) were programmed as user defined presets. This flexibility allows for the use of this algorithm within other data sets regardless of the initial data resolution.

2.4. Data analysis

In accordance with the snow measurement assumptions (Section 2.2), snow interception (in mm SWE) can then be thought of as: SWE in the open (P_{open}) − SWE in the forest (SWE_{forest}). In order to normalize the data over each storm event, the ratio of SWE_{forest}/P_{open} was used as a direct comparison to the metrics from the ALS data. This included all metrics seen within Table 2 as well as the LAI, CC, and incoming solar radiation generated from synthetic ALS images (Section 2.3.2). All metrics were individually correlated to the interception data at each storm event and subsequently averaged.

All forest metrics were then inter-compared using correspondence analysis (CA) in order to analyze cross-correlation between the metrics. CA is a non-parametric principle component method for analyzing correspondence or independence among variables. The significance of each association was based upon the chi-squared distance between each data point and the expected value, where the expected value was equal to the value that has the highest probability of occurring within the dataset (Car, 2002). Eigenvectors (factors) associated with the Eigen decomposition of the matrix of the chi-square values from the data set were plotted on independent axes, along with the Eigen values for each sample which allowed for a visual assessment of independence or cross correlation. Each factor axes were also assigned a significance value (percent of inertia) which represented an estimate of the amount of variability captured within the dataset from the factor. Independence was then analyzed by the plotted variable separation distance, with greater significance given to the separation on the axes with a higher factor value (Greenacre and Blasius, 1994; Lorenzo-Seva et al., 2009; Van de Velden and Kiers, 2003, 2005).

K means clustering was then used in order to automatically choose groups of variables which have similar CA plotting characteristics by maximizing the inter cluster distance and minimizing the intra cluster distances (Seber, 1984; Späth, 1985). Independence within CA is normally qualitatively analyzed from a visual analysis of variable separation. However, this unique method pairing (CA and *K* means clustering) allowed for an automated and unbiased approach. The analysis was performed iteratively from a random centroid selection of each potential cluster (cluster groups set to 4). The factor values from the CA were also integrated into the *K* means clustering routine, where the partitioning of the intra and inter clustering distances were further based on the factor value (refer to axis values in Fig. 5). Each factor value was given a normalized percent weight based on the additive of each plotted dimension factor value (3 dimensions). These weights were then applied to the coordinates of the input data. This allowed the *k* means clustering routine to favor relationships based upon the amount of variance captured within each dimension (percent of inertia).

3. Results and discussion

Table 3 gives an overview of correlations of canopy metrics to interception ratio. All gap diameter metrics retained almost exact correlations as the distance to canopy metrics. Due to this, the gap diameter metrics have been removed from Table 3. This highlights the near identical predictive ability of these two metrics and shows that mean gap diameter represents, regardless of the quadrant, almost equivalent gap opening characteristics as mean distance to canopy. Furthermore, all maximum and minimum estimates (max/min distance to canopy, max/min gap diameter for the entire domain as well as sectors) demonstrated significantly lower correlations to the interception rate as compared to mean (mean distance to canopy, mean gap diameter) or total gap area estimates. Therefore all metrics quantifying maximum or minimum length regardless of the quadrant have also been removed from Table 3. This implies that even if there are large fetches within a specific direction where there is no canopy, the influence to snow interception is minimal. The descriptors which integrate all directions within a sector are better apt at interception estimation than canopy metrics which hold true only for specific directions. However, estimations of such metrics (max/min distance to canopy, max/min gap diameter) could prove important for other factors within the energy balance valuable for forest snow modeling that are not analyzed in this study such as radiation transfer.

The highest correlated metric was mean distance to canopy and maintained this ranking (average $R = 0.78$, standard deviation = 0.09) within each precipitation event (correlation range = 0.58–0.89). Canopy closure had a slightly reduced average correlation (−6%) at 0.72 and demonstrated a slightly higher standard deviation with a correlation range between 0.43 and 0.87. LAI showed significantly lower correlations than the higher correlated metrics, with an average *R* of 0.57, standard deviation of 0.16 and a correlation range between 0.21 and 0.77. The best correlated area metric was total gap area which shared an equivalent average correlation with canopy closure at 0.72 and a slightly reduced standard deviation of 0.11 (correlation range = 0.50–0.86). These results imply that metrics which evaluate the overall position of a point in space (mean distance to canopy), as well as metrics which calculate larger scale features (total gap area),

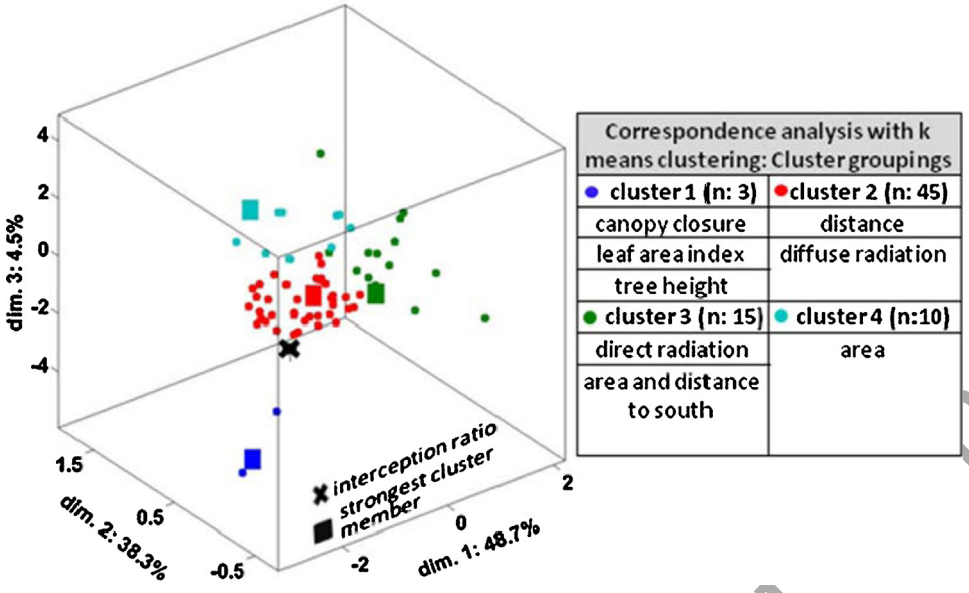

Fig. 5. Correspondence analysis with integrated *k* means clustering of metrics for 4 groupings. Each grouping is represented by a color, and within each grouping a box shows the location of highest correlated metric within the grouping. The cross represents the location of the independent element, snow interception ratio. The traditional canopy descriptors, CC and LAI and the mean tree height proxy were plotted in the same grouping, showing a high degree of cross correlation between these descriptors. The second largest grouping in light blue integrated only estimates of area. The third cluster included direct radiation estimates as well as area and distance estimates to the south. The largest cluster (red) integrated all remaining distance estimators and included the highest correlated factor of the series, mean distance to canopy.

are equally important for interception estimation as the canopy parameters which evaluate just overlying canopy density above a point. An overview of the metric statistics can be seen in Table 3.

The correspondence and *k* means analysis shown in Fig. 5 utilized a compilation of all storm events. However, similar results were also observed when the analysis was run on individual storm events. The smallest cluster ($n = 3$) retained canopy closure, leaf area index and tree height proxies. The tight clustering of these parameters demonstrated a significant amount of cross-correlation (dependence) between these metrics and implied that regardless of the metric, they represented identical parts of the total interception variation. The strongest (highest correlation to interception) member of this grouping was tied at mean tree height and canopy closure with the lowest correlated end member being leaf area index. This implied that not only may LAI not be the best predictor for interception, but regardless of which of these metrics are used, identical parts of the total interception variation are represented.

The second smallest cluster ($n = 10$) integrated all total gap area metrics (total gap area, gap area to the north 180°, gap area to the northeast 90°, etc.) except those to a southerly direction, with the strongest member being total gap area. This demonstrates the potential utility of a canopy metric which represents a larger scale feature such as canopy and forest openings.

The next grouping ($n = 15$) incorporated all distance to the south estimates (mean distance to canopy - southeast 90°, etc southeast 90°, etc– south 180°, mean distance to canopy – southeast 90°, etc.), area to the south estimates (mean gap area – south 180°, mean gap area – southeast 90°, etc.), and all incoming solar radiation estimates which incorporated the direct component (direct incoming solar radiation – DIR_IR and average daily potential incoming solar radiation – PISR). The strongest member was average daily potential incoming solar radiation (PISR). This does not necessary imply that solar radiation is an important factor within interception modeling, this does however highlight the interplay between canopy openness and solar radiation, and shows that perhaps area measurements to the south could be used as a solar radiation proxy when no direct estimates are available for snow melt studies.

The largest grouping ($n = 45$) incorporated all distance estimates (mean distance to canopy, mean distance to canopy – north 180°, mean distance to canopy – northeast 90°, etc.) except those with a southern aspect as well as all diffuse incoming radiation estimates (DIF_IR). The strongest end member in this grouping, mean distance to canopy also had the highest overall correlations of all analyzed metrics and maintained low variance for all storm events. These correspondence results in tandem with the correlation analysis highlight that metrics which analyze the overall position of a point within a gap relative to the canopy, are equally, if not more important for interception modeling, than just a canopy coverage assessment.

Finally, the metric correspondence analysis demonstrated that no increased predictive power is available within this dataset if LAI and CC are used simultaneously for snow interception estimates. It further highlighted the weak direct correlation between LAI and snow interception ratio. Several of the variables created from the searching algorithm demonstrated significantly higher correlations than LAI and showed distinct separation from the traditional metrics grouping (cluster 1). This implied that not only could a variable such as a mean distance to canopy accurately be used as an independent variable to model interception ratio but also that a composite of these variables could create a more robust model than the standard pairing of LAI and canopy closure. Current interception models, either stand alone, or subsequently integrated into snow melt models use this standard metric pairing. Therefore, it seems likely that one or more of the new metrics could be integrated into the interception model distributions for a more accurate representation of the overall water balance within forested areas.

4. Conclusion

ALS has the potential to supplement not just interception modeling techniques but also forest snow modeling in general. Within the field areas surrounding Davos, Switzerland, the availability of ALS data has allowed for the creation of novel canopy metrics without the prohibitive time necessary to manually measure thousands of points to describe the canopy over large areas. The vector

searching algorithm is fully automated and could characterize thousands of locations within the field areas (Section 2.1) in a period of minutes. This, in conjunction with an extensive database of manually measured snow interception over heterogeneous terrain (~8500 manual measurement points) allowed us to create and test the capabilities of new input metrics in relation to parameters historically used for forest snow modeling (CC and LAI).

LAI demonstrated low correlations when directly compared to snow interception ratio and further showed a large cross-correlation with canopy closure. Mean distance to canopy had the highest correlation over all storm events to the interception ratio. But in contrast to LAI, this variable did not show any cross correlation with canopy closure (CC). Likewise, total gap area, an indirect measurement of apparent gap fraction also showed a high correlation to interception ratio without demonstrating a significant cross-correlation to CC or to mean distance to canopy.

These findings suggest that modeling forest snow processes with both CC and LAI may not be the best option due to both the low correlation of LAI as well as high cross-correlation between these variables. However, the pairing of mean distance to canopy and/or total gap area with canopy closure could give more robust estimations of snow interception within heterogeneous terrain. Together, these variables have the ability to quantify not just canopy density but canopy metrics relative to larger scale canopy structural features such as canopy openings.

In order to permit for more robust modeling at scales greater than the point scale, the greater canopy topography needs to be accounted for. The inclusion of metrics which describe point based canopy topography (canopy closure) with those which give information regarding where these metrics reside in relation to the larger encompassing features such as total gap area or mean distance to canopy could allow for better upscaling of snow forest models to the landscape scale.

All programming was performed using Matlab. All scripts related to this algorithm are freely available upon request.

Acknowledgements

This project was funded by the Swiss National Science Foundation (SNF – project 200021_146184/1). Field help was given by Dr. Florian Kobierska, Clare Webster, Nena Griessinger, Saskia Gindraux, Franziska Zieger, Franziska Zahner, Jiri Roubinek, and Mathias Rieckh of the WSL Institute for Snow and Avalanche Research SLF, snow hydrology group. Programming support was given by Dr. Jan Magnusson, also of the snow hydrology group. Further statistical analysis help was given from the aid of Dr. Jim Car of the University of Nevada, Reno. Editing help was given by Dr. Chris Hoyle from the Paul Scherrer Institute.

References

Asner, G.P., Mascaro, J., Muller-Landau, H.C., et al., 2011. A universal airborne LiDAR approach for tropical forest carbon mapping. Oecologia 168 (4), 1147–1160.
Breda, N., 2003. Ground-based measurements of leaf area index: a review of methods, instruments and current controversies. J. Exp. Bot. 54 (392), 2403–2417.
Car, J., 2002. Data Visualization in the Geological Sciences. Prentic Hall, Upper Saddle River, NJ.
Chang, 2003. Forest Hydrology: An Introduction to Water and Forests. CRC Press, Boca Raton, 392 pp.
Essery, R., Pomeroy, J., 2001. Soil-vegetation-atmosphere transfer schemes and large-scale hydrological models. In: International Association of Hydrological Science Conference, Maastricht, Netherlands, pp. 343–347.
Essery, R., Pomeroy, J., Parviainen, J., Storck, P., 2003. Sublimation of snow from coniferous forests in a climate model. J. Clim. 16, 1855–1864.
Essery, R., Pomeroy, J., Baxter, R., et al., 2009. SNOWMIP2 an evaluation of forest snow process simulations. Bull. Am. Meteorol. Soc., 1120–1135.
Fleck, S.R.S., Cater, M., Schleppi, P., Ukonmaanaho, L., Greve, M., Hertel, C., Weis, W., Rumpf, S., 2012. Manual on methods and criteria for harmonized sampling, assesment, monitoring and analysis of the effects of air pollution on forests: Part XVII, leaf area measurements. In: United Nations Economic Commission for Europe International Co-operative programme on Assesment and Monitoring of Air Pollution Effects on Forests. ICP Forests, Hamburg.
Golding, D.L., Swanson, R.H., 1986. Snow distribution in clearings and adjacent forest. Water Resour. Res. 22 (13), 1931–1940.
Greenacre, M., Blasius, J., 1994. Correspondence Analysis in the Social Sciences. Academic Press, Waltham, MA, 370 pp.
Guntner, A., Stuck, J., Werth, S., et al., 2007. A global analysis of temporal and spatial variations in continental water storage. Water Resour. Res. 43 (5).
Hedstrom, N.R., Pomeroy, J., 1998. Measurements and modelling of snow interception in the boreal forest. Hydrol. Process. 12 (10–11), 1611–1625.
Hyer, E.J., Goetz, S.J., 2004. Comparison and sensitivity analysis of instruments and radiometric methods for LAI estimation: assessments from a boreal forest site. Agric. For. Meteorol. 122 (3–4), 157–174.
Koivusalo, H., Kokkonen, T., 2002. Snow processes in a forest clearing and in a coniferous forest. J. Hydrol. 262, 145–164.
Korhonen, L., Morsdorf, F., 2014. Estimation of canopy cover, gap fraction and leaf area index with airborne laser scanning. In: Maltamo, M., Naesset, E., Vauhkonen, J. (Eds.), Forestry Applications of Airborne Laser Scanning: Concepts and Case Studies. Springer, Science and Business Media, Dordrecht, p. 464.
Lorenzo-Seva, U., Van de Velden, M., Kiers, H., 2009. Oblique rotation in corrrespondence analysis: a step forward in search of the simplest interpretation. Br. J. Math. Stat. Psychol. 62, 583–600.
Lovell, J.L., Jupp, D.L.B., Culvenor, D.S., et al., 2003. Using airborne and ground-based ranging lidar to measure canopy structure in Australian forests. Can. J. Remote Sens. 29 (5), 15.
Lundberg, A., Halldin, S., 2001. Snow interception evaporation – rates, processes and measurement techniques. Theor. Appl. Climatol. 70, 117–133.
Moeser, D., Roubinek, J., Schleppi, P., et al., 2014. Canopy closure, LAI and radiation transfer from airborne LiDAR synthetic images. Agric. For. Meteorol. 197, 158–168.
Montesi, J., Elder, K., Schmidt, R.A., Davis, R.E., 2003. Sublimation of intercepted snow within a subalpine forest canopy at two elevations. J. Hydrometeorol. 5 (5), 763–773.
Morsdorf, F., Meier, E., Kötz, B., et al., 2004. LIDAR-based geometric reconstruction of boreal type forest stands at single tree level for forest and wildland fire management. Remote Sens. Environ. 92 (3), 353–362.
Morsdorf, F., Kötz, B., Meier, E., et al., 2006. Estimation of LAI and fractional cover from small footprint airborne laser scanning data based on gap fraction. Remote Sens. Environ. 104 (1), 50–61.
Morsdorf, F., Frey, O., Meier, E., et al., 2008. Assessment of the influence of flying altitude and scan angle on biophysical vegetation products derived from airborne laser scanning. Int. J. Remote Sens. 29 (5), 1387–1406.
Pomeroy, J., Gray, D.M., Shook, K., et al., 1998a. An evaluation of snow accumulation and ablation processes for land surface modeling. Hydrol. Process. 12, 2339–2367.
Pomeroy, J.W., Parviainen, J., Hedstrom, N., Gray, D.M., 1998b. Coupled modelling of forest snow interception and sublimation. Hydrol. Process. 12, 2317–2337.
Riaño, D., Valladares, F., Condés, S., Chuvieco, E., 2004. Estimation of leaf area index and covered ground from airborne laser scanner (Lidar) in two contrasting forests. Agric. For. Meteorol. 124 (3–4), 269–275.
Rutter, N., Essery, R., Pomeroy, J., et al., 2009. Evaluation of forest snow processes models (SnowMIP2). J. Geophys. Res. 114 (D6).
Satterlund, D., Haupt, H., 1967. Snow catch by conifer crowns. Water Resour. Res. 3 (4).
Schmidt, R.A., Gluns, D., 1991. Snowfall Interception on branches of three conifer species. Can. J. For. Res. 21, 1262–1269.
Seber, G.A.F., 1984. Multivariate Distributions, in Multivariate Observations. John Wiley & Sons, Inc., Hoboken, NJ, USA.
Solberg, S., Brunner, A., Hanssen, K., et al., 2009. Mapping LAI in a Norway spruce forest using airborne laser scanning. Remote Sens. Environ. 113 (11), 2317–2327.
Solberg, S., 2010. Mapping gap fraction, LAI and defoliation using various ALS penetration variables. Int. J. Remote Sens. 31 (5), 1227–1244.
Späth, H., 1985. Cluster Dissection and Analysis: Theory, FORTRAN Programs, Examples. Horwood.
Storck, P., Lettenmaier, D.P., Bolton, S.M., 2002. Measurement of snow interception and canopy effects on snow accumulation and melt in a mountainous maritime climate, Oregon, United States. Water Resour. Res. 38 (11), 16.
Thimonier, A., Sedivy, I., Schleppi, P., 2010. Estimating leaf area index in different types of mature forest stands in 516 Switzerland: a comparison of methods. Eur. J. For. Res. 129, 543–562.
Troendle, C.A., Meiman, J.R., 1986. The effect of patch clearcutting on the water balance of a subalpine forest slope. In: 54th Annual Western Snow Conference, Phoenix, AZ.
US Army Corps of Engineers, 1956. Snow Hydrology: Summary Report of the Snow Investigations. North Pacific Division, Portland, OR, pp. 437.
Van de Velden, M., Kiers, H., 2003. An application of rotation in correspondence analysis. In: New Developments in Psychometrics. Springer, Tokyo, Japan, pp. 471–478.
Van de Velden, M., Kiers, H., 2005. Rotation analysis in correspondence analysis. J. Classif. 22 (2), 251–271.
Varhola, A., Coops, N., Bater, C., et al., 2010a. The influence of ground- and lidar-derived forest structure metrics on snow accumulation and ablation in disturbed forests. Can. J. For. Res. 40 (4), 812–821.

Varhola, A., Coops, N., Weiler, M., et al., 2010b. Forest canopy effects on snow accumulation and ablation: an integrative review of empirical results. J. Hydrol. 392 (3–4), 219–233.
Veatch, W., Brooks, P.D., Gustafson, J.R., et al., 2009. 'Quantifying the effects of forest canopy cover on net snow accumulation at a continental, mid-latitude site'. Ecohydrology 2 (2), 115–128.
Winkler, R.D., Spittlehouse, D.L., Golding, D.L., 2005. Measured differences in snow accumulation and melt among clearcut, juvenile, and mature forests in southern British Columbia. Hydrol. Process. 19 (1), 51–62.
Zhao, K., Popescu, S., Meng, X., et al., 2011. Characterizing forest canopy structure with lidar composite metrics and machine learning. Remote Sens. Environ. 115 (8), 1978–1996.
Zhang, Y., Chen, J.M., Miller, J.R., 2005. Determining digital hemispherical photograph exposure for leaf area index estimation. Agric. For. Meteorol. 133 (1–4), 166–181.